Monitoring Vegetation Cover Changes in the Darmian and Sarbisheh Protected Area Using Satellite-derived Vegetation Indices in Google Earth Engine Platform

Hassan Davoudi[1], Elham Yousefi[2,*], Saeid Gholinejad[3]

1- MSc in Land use planning, Department of environment, Faculty of natural resources and environment, University of Birjand, Birjand, Iran. ORCID ID: 0009-0001-3386-2972
2- Associate Professor, Department of Environment, Drought and Climate Change Research Group, Faculty of Natural Resources and Environment, University of Birjand. Iran. ORCID ID: 0000-0002-5396-6402.
3- Assistant Professor, Department of Surveying Engineering, Faculty of Civil and Surveying Engineering, Graduate University of Advanced Technology, Kerman, Iran.

***Corresponding Author:** E_yusefi_31@birjand.ac.ir

Abstract

Drought is considered one of the most significant natural hazards in protected areas; therefore, monitoring its impacts on these regions can contribute substantially to their effective management. Accordingly, this study investigated drought trends in the Darmian and Sarbisheh Protected Areas during the period 2000–2022 using satellite data within the Google Earth Engine platform. To this end, meteorological drought conditions were first assessed using climatic-meteorological variables, including the Standardized Precipitation Index (SPI) derived from CHIRPS and soil moisture from the SMAP satellite. Subsequently, changes in vegetation cover were evaluated through time-series analysis of vegetation indices extracted from MODIS satellite imagery, including the Normalized Difference Vegetation Index (NDVI), Enhanced Vegetation Index (EVI), Vegetation Condition Index (VCI), Temperature Condition Index (TCI), Vegetation Health Index (VHI), and Standardized Vegetation Index (SVI). The Mann–Kendall test applied to the vegetation cover area time series indicated a statistically significant increasing trend ($Z = 8.96$, $p < 0.001$, $\tau = 0.27$), while Sen's slope estimated an average increase of 27.26 area units per observation over the study period. This increasing trend was also reflected in the vegetation index time series. The results indicated that, while the monthly SPI exhibited a decreasing trend and soil moisture showed a relatively stable trend, both suggesting an intensification of meteorological drought in the region, the vegetation indices displayed a relatively increasing trend. The significant differences observed between areas inside and outside the protected boundary confirm the effectiveness of conservation measures, such as restrictions on livestock grazing and control of human exploitation, in mitigating drought severity.

Keywords: Darmian and Sarbisheh Protected Area; Drought; Satellite Images; Vegetation Index; Google Earth Engine (GEE)

Pre-publication Version

Introduction

Drought is an inherent natural phenomenon in the climate of arid and semi-arid regions, such as Iran, which results in extensive environmental, economic, and social consequences. The intensity and duration of drought vary depending on the climatic conditions and specific characteristics of each region. Its effects become rapidly apparent on vegetation cover, water resources, and human activities, particularly in areas with limited water resources. (Du et al., 2013; Romiyani et al., 2020). Drought is defined as a period during which precipitation or soil moisture falls below the long-term regional average. This phenomenon does not necessarily imply permanent dryness; rather, it represents a temporary climatic anomaly that can also occur in non-arid regions. (Herring et al., 2015; Linsley & Franzini, 1981). The World Meteorological Organization identifies precipitation, temperature, soil moisture, and evapotranspiration as the primary factors influencing drought occurrence.

There are several natural factors causing drought, such as the El Niño phenomenon and solar variations, as well as human activities like the increase in greenhouse gases, which induce changes in global precipitation patterns and temperatures. (Omidvarpour & Goudarzi, 2019; Yazdani & Zareh-Abiyaneh, 2011). Drought also has numerous direct and indirect effects, including reduction in agricultural products, declining groundwater levels, habitat destruction, unemployment, and migration. (Farajzadeh, 2005; Rezaei et al., 2012). Wilhite has classified this phenomenon into four main types: meteorological, agricultural, hydrological, and socio-economic drought. (Wilhite, 2000). The first type commences with a reduction in precipitation, while the second is associated with diminished soil moisture and crop damage. The third type of drought involves a decrease in surface and groundwater resources, and the fourth refers to long-term economic and social consequences. (Abonouri, 2008; Alipour et al., 2013).

Monitoring changes in vegetation cover and drought indices in arid and semi-arid regions is of critical importance, as such understanding can support optimal natural resource management and ecosystem conservation. (Alonso et al., 2016). Given Iran's predominantly arid climate, low annual precipitation, and recurrent drought events, investigating drought dynamics is particularly important, especially in the eastern regions of the country. Recent droughts have resulted in reduced vegetation cover, declining agricultural productivity, and increased population migration in these areas. (Alavi-Panah, 2006; Delfiyan et al., 2021).

In recent years, satellite-based data have been increasingly employed in drought monitoring studies. The application of these data, particularly through cloud-based platforms such as Google Earth Engine (GEE), enables the evaluation of drought indices over large spatial and temporal extents with high accuracy and relatively low computational and financial costs. Numerous studies have demonstrated that drought exerts a direct influence on vegetation cover; consequently, remote sensing–derived vegetation indices constitute effective indicators for drought monitoring in arid and semi-arid environments. Rahnama et al. (2022), Shokrian et al. (2022), Rashtbari et al. (2020), and Karimi et al. (2020) reported strong correlations between remotely sensed vegetation indices—including the Normalized Difference Vegetation Index (NDVI), Soil-Adjusted Vegetation Index (SAVI), Simple Ratio (SR), and Vegetation Condition Index (VCI)—and meteorological drought indices. Furthermore, studies by Saedian and Shafiezadeh-Moghadam (2021) and Zareh Khormizi and Ghaffarian Malmiri (2020) confirmed the high efficiency of GEE for analyzing spatio-temporal changes in vegetation cover.

Numerous studies have employed the integration of vegetation and meteorological indices within the GEE platform for drought monitoring purposes. Veneros and García (2021) evaluated drought management in Peru using the Standardized Vegetation Index (SVI) implemented in GEE. Zhao et al. (2022) compared multiple drought indices in the Shaanxi–Gansu–Ningxia region over the period 2003–2020 using the GEE environment and successfully analyzed the spatiotemporal dynamics of drought with high accuracy. Similarly, Fakhar and Kaviani (2024) monitored and assessed drought conditions in the Qazvin Plain using indices derived from MODIS imagery within the GEE platform. In a comparable study, drought characteristics were analyzed in the Chi River basin during 2001–2020 based on MODIS data processed in GEE. (Suwanlee et al., 2025). The findings of the latter two studies demonstrated that the concurrent use of vegetation and climatic data within the GEE framework enables rapid, continuous, and reliable drought monitoring at both regional and global scales.

In addition, Tabassum and Khan (2024) conducted a comparative analysis of drought indices in GEE, showing that certain indices exhibit superior performance in detecting both short-term and long-term drought events. Collectively, these studies emphasize that the integration of vegetation-based and

Pre-publication Version

climate-based indices within the GEE environment provides an effective tool for drought monitoring and management across diverse geographical regions.

Most existing studies in arid regions tend to focus on broad agricultural zones or generic administrative boundaries. There is a notable paucity of research focusing on protected areas—regions that are ecologically fragile and serve as biodiversity hotspots. Accordingly, the present study applies remote sensing data within the GEE platform to analyze the spatiotemporal variations of vegetation cover in response to drought in the Darmian and Sarbisheh Protected Area. This region, characterized by a high diversity of natural features, provides habitat for various wildlife species and has been designated as a protected area under the supervision of the Iranian Department of Environment since 2018. The ecological significance of the study area, from both vegetation and wildlife perspectives, underscores the necessity of assessing and monitoring drought-induced impacts. Protected areas in arid environments, such as the Darmian and Sarbisheh region, face unique pressures where drought-induced vegetation loss directly threatens wildlife habitats and conservation efforts.

In this research, trends in climatic and meteorological variables, including the Standardized Precipitation Index (SPI) and soil moisture, as well as vegetation indices—namely the Normalized Difference Vegetation Index (NDVI), Vegetation Condition Index (VCI), Temperature Condition Index (TCI), Vegetation Health Index (VHI), and Standardized Vegetation Index (SVI)—are extracted for the period 2000–2022, all using the GEE environment. The climatic and meteorological variables are used to characterize meteorological drought conditions in the region, whereas the vegetation indices reflect vegetation responses to drought stress. The outcomes of this study can provide a scientific basis for developing management strategies and supporting decision-making processes related to natural resource conservation and biodiversity protection, particularly in the Darmian and Sarbisheh Protected Area.

In general, unlike prior regional studies that treat land cover changes as uniform, our work offers three primary contributions:

- We move beyond standard agricultural monitoring by focusing on a protected habitat, where the ecological stakes—specifically wildlife survival—are higher than in crop-based studies.
- By analyzing distinct climatic and vegetation indices (SPI, NDVI, VCI, TCI, VHI, SVI, and soil moisture) within the GEE framework, we provide a holistic view of drought stress that captures both the meteorological drivers and the biological responses of the ecosystem.
- By analyzing the 2000–2022 period, we generate a long-term trajectory of the region's response to recurrent droughts, offering a baseline for future management that has not previously existed for this specific protected area.

The remainder of this paper is organized as follows. Section 2 describes the study area, the remote sensing datasets employed, and the satellite-derived indices used in the analysis. Section 3 presents and discusses the results, focusing on the spatiotemporal trends of climatic–meteorological variables and vegetation cover, as well as index-based maps illustrating changes in vegetation conditions. Finally, Section 4 summarizes the main conclusions of the study and outlines directions for future research.

Materials and Methods

Study Area

The Darmian and Sarbisheh Protected Area, covering approximately 58,777 ha, is located in South Khorasan Province, Iran, and extends between 59°40′–60°02′ E longitude and 32°34′–32°58′ N latitude. The geographical location of the study area is illustrated in Fig 1. The region has a mean elevation of approximately 1,950 m above sea level, with an average annual temperature ranging from 15.9 to 25 °C and a mean annual precipitation of about 170 mm. The climate is classified as arid to semi-arid, and the dominant vegetation cover consists primarily of steppe and shrubland communities.

The prevailing landform is characterized by elevated hilly terrain with moderate to steep slopes, and the physiography includes numerous valleys and seasonal drainage channels. Surface water resources comprise springs, qanats, and ephemeral rivers, whose spatial distribution plays a crucial role in shaping wildlife habitat patterns. The area supports a significant population of the eastern Iranian urial sheep (*Ovis vignei*), and conservation efforts targeting this species have contributed to the protection of other flagship fauna, including Pallas's cat (*Otocolobus manul*), the stone marten (*Martes foina*), and several raptor species (Supreme Council of Environmental Protection Resolution No. 284, 2007).

Pre-publication version

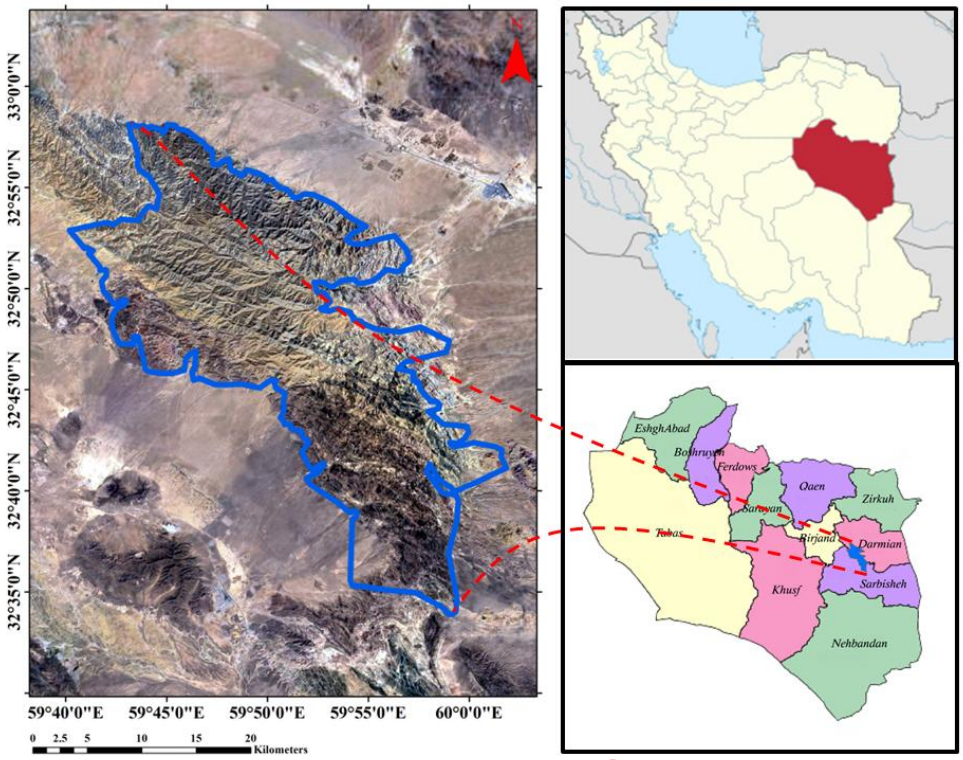


Fig 1. Location of the Darmian and Sarbisheh protected area (blue line boundary), South Khorasan Province, Iran.

Satellite Data

To investigate the impacts of drought in the study area, the period from 2000 to 2022 was selected for analysis. Two categories of satellite-based time series data were employed: climatic–meteorological datasets and vegetation indices. It should be noted that all datasets used in this study, as well as the associated processing procedures, were implemented entirely within the GEE platform. The information on the applied datasets is shown in Table 1.

Table 1. Information on the applied datasets on the GEE platform.

Data	GEE Package	Band Name	Spatial Resolution (m)	Temporal Resolution
Rainfall	UCSB-CHG/CHIRPS/DAILY	'precipitation'	5600	Daily
Soil Moisture	NASA/SMAP/SPL4SMGP/008	'sm_surface' 'sm_rootzone'	11000	3-hourly
Vegetation Index	MODIS/061/MOD13Q1	'NDVI'	250	16-day
LST	MODIS/061/MOD11A1	'LST_Day_1km'	1000	Daily

The climatic–meteorological datasets consist of time series of precipitation data and surface and sub-surface soil moisture data. These datasets provide valuable information for characterizing meteorological drought conditions in the region. Precipitation time series were derived from the CHIRPS satellite dataset, based on which the SPI was calculated. The SPI, first introduced by McKee et al. (1993) for monitoring meteorological drought, is among the most widely used drought indices in drought analysis studies (Abd-Elhamid et al., 2024; Bagale et al., 2024; Bouaziz et al., 2021; Liu et al., 2018; Qaisrani et al., 2021). Its widespread application is primarily attributed to its computational simplicity, the broad availability of precipitation data, and its flexibility for calculation across multiple temporal scales. The Standardized Precipitation Index (SPI) is calculated for meteorological drought monitoring based on the anomaly of precipitation relative to the long-term behavior of the same region. To calculate it, first the total precipitation on a specific time scale, such as 1, 3, 6, or 12 months, is extracted from a long-term statistical period. Then, an appropriate statistical distribution, usually the gamma distribution, is fitted to the precipitation data, and the cumulative probability of the observed precipitation is calculated. In the next step, this probability is converted to a standard normal distribution

Pre-publication

with a mean of zero and a standard deviation of one. The final SPI value indicates how many standard deviations the observed precipitation is away from normal conditions; negative values indicate drought and positive values indicate wetness. Typically, values less than -1 are considered moderate drought, less than -1.5 are considered severe drought, and less than -2 are considered very severe drought. Table 2 presents the classification of drought severity based on SPI values.

Table 2. Drought-severity classification based on SPI values (McKee et al., 1993).

SPI Value	Category of Drought
≥ 2	Extremely Wet
$1.5 - 1.99$	Very Wet
$1 - 1.49$	Moderately wet
$-0.99 - 0.99$	Mild Drought
$-1.49 - -1$	Moderate Drought
$-1.99 - -1.5$	Severe Drought
≤ -2	Extreme Drought

Surface and sub-surface soil moisture data were obtained from the Soil Moisture Active Passive (SMAP) satellite mission. It should be noted that SMAP was launched in January 2015 and became operational in April 2015; consequently, soil moisture data are not available for the entire 22-year study period. Accordingly, soil moisture time series were extracted for the period 2015–2022. Although this time span covers only seven years, the analysis provides valuable insights into temporal trends in soil moisture conditions within the study area.

Along with the climatic–meteorological variables, vegetation indices were employed to assess vegetation conditions in the study area. It should be noted that, to achieve a more comprehensive understanding of vegetation dynamics, multiple vegetation indices were utilized rather than relying on a single index. The first applied vegetation index is the NDVI, which was originally introduced by Tucker (1979) and has since been widely used in remote sensing studies of vegetation. This index is calculated using the red and near-infrared spectral bands as follows. (Tucker, 1979):

$$\mathrm{NDVI} = \frac{\rho_{NIR} - \rho_R}{\rho_{NIR} + \rho_R} \tag{1}$$

Notably, this study utilized the NDVI band from the MODIS MOD13Q1 product, which was also employed to calculate the other subsequent indices.

The VCI is another index applied in this study. (Kogan, 1995b). VCI is a normalized index based on the temporal variability of NDVI and is widely used to assess vegetation stress and drought severity (Barrett et al., 2020; Jiao et al., 2016; Quiring & Ganesh, 2010; Zambrano et al., 2016). By minimizing the effects of seasonal variability, this index enables the evaluation of vegetation health trends across different temporal scales. The VCI is calculated using the following equation:

$$\mathrm{VCI}_i = \frac{\mathrm{NDVI}_i - \mathrm{NDVI}_{\mathrm{Min}}}{\mathrm{NDVI}_{\mathrm{Max}} - \mathrm{NDVI}_{\mathrm{Min}}} \tag{2}$$

In the above equation, $\mathrm{NDVI}_{\mathrm{Max}}$ and $\mathrm{NDVI}_{\mathrm{Min}}$ represent the maximum and minimum NDVI values for the corresponding month over the study period, respectively, and VCI_i denotes the vegetation condition for month i. The VCI ranges from 0 to 1, where values close to 0 indicate poor vegetation growth and severe drought conditions, whereas values approaching 1 reflect favorable vegetation status.

The TCI is also employed in this study, originally proposed by Kogan (1995a). This index is based on the fact that canopy or soil surface temperature increases with increasing water stress under high-temperature conditions, which are typically associated with reduced vegetation cover or depleted soil moisture. The occurrence and development of drought are therefore closely linked to land surface temperature. Increasing land surface temperatures during the growing season indicate unfavorable or drought conditions, whereas lower surface temperatures reflect healthier environmental conditions.

Pre-Publication Version

Derived from thermal infrared data, the TCI has been widely used for drought monitoring and can be calculated using the following equation:

$$\mathrm{TCI}_i = \frac{\mathrm{LST}_{\mathrm{Max}} - \mathrm{LST}_i}{\mathrm{LST}_{\mathrm{Max}} - \mathrm{LST}_{\mathrm{Min}}} \quad (3)$$

Where $\mathrm{LST_i}$ presents the land surface temperature in month i, while $\mathrm{LST_{Max}}$ and $\mathrm{LST_{Min}}$ denote the maximum and minimum monthly land surface temperature values over the study period, respectively. Accordingly, TCI_i indicates the temperature condition for month i.

Another applied index in this study is the VHI, which integrates the two previously mentioned TCI and VCI indices. (Kogan, 1995a, 1997). The VCI and TCI reflect vegetation moisture conditions and thermal stress, respectively. Consequently, TCI serves as a complementary indicator to VCI for drought monitoring, and when used jointly, these indices provide a useful tool for assessing vegetation productivity. The VHI is calculated as follows:

$$\mathrm{VHI_i} = \frac{\mathrm{TCI_i} + \mathrm{VCI_i}}{2} \quad (4)$$

Assuming other environmental conditions are near normal, in the VHI framework, vegetation is more sensitive to moisture availability during canopy development (leaf emergence) and to temperature during the flowering stage. Since the relative contributions of moisture and temperature throughout the plant growth cycle are unknown, equal weights are assigned to VCI and TCI in the computation of VHI. Time-series analysis of composite indices such as VHI is particularly effective for distinguishing between short-term (temporary) and long-term (chronic) drought conditions.

The last applied vegetation index is SVI. This index calculates the probability of variation in a certain vegetation index (VI) in a pixel location with respect to the normal value of that VI. (Peters et al., 2002). To calculate it, first the z-score for each pixel location should be determined through the following equation:

$$\mathrm{z}_{ijk} = \frac{\mathrm{VI}_{ijk} - \mu_{ij}}{\sigma_{ij}} \quad (5)$$

where z_{ijk} is the z-value for pixel i during week j for year k, VI_{ijk} is the weekly VI for pixel i during week j for year k, and μ_{ij} and σ_{ij} are the mean and standard deviation of VI for pixel i during week j over n years, respectively. Since z_{ijk} assumed to fit a standard normal distribution, its probability density function is obtained as follows:

$$\mathrm{SVI} = \mathrm{P}(Z < z_{ijk}) \quad (6)$$

Although SVI was introduced based on NDVI (Peters et al., 2002), it is possible to use another VI in the formula, such as EVI (Veneros & García, 2021).

Pre-publication Version

Results and Discussion

Climatic-Meteorological Variables Analysis

In this section, the results of the time-series analysis of the SPI and soil moisture data are evaluated. Examination of these two parameters provides valuable insights into meteorological drought conditions in the study area.

The time series of the six-month SPI values derived from the CHIRPS satellite dataset for the study area is illustrated in Fig 2. Analysis of this time series, based on the drought classification presented in Table 2, indicates a declining trend in SPI values over the 22 years, reflecting the occurrence and intensification of meteorological drought conditions in the region. Furthermore, Fig 3 depicts the spatial

distribution of the SPI across the study area. In this figure, white colors represent positive SPI values, indicating areas where precipitation exceeds the long-term mean.

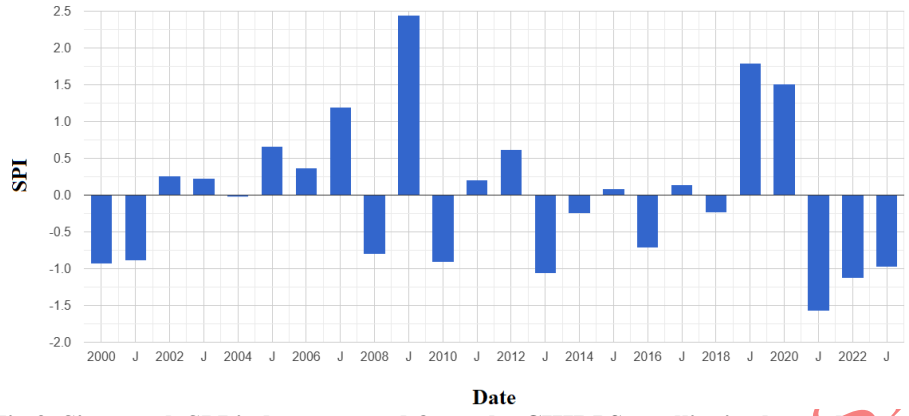


Fig 2. Six-month SPI index extracted from the CHIRPS satellite in the study area.

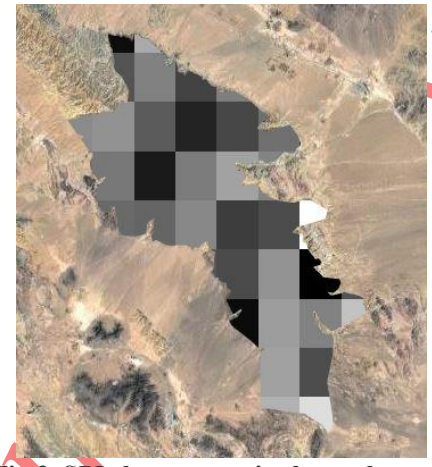


Fig 3. SPI change map in the study area.

The temporal variations of soil moisture in the study area derived from SMAP satellite data are presented in Fig. 4 In this figure, the red curve represents sub-surface soil moisture, while the blue curve corresponds to surface soil moisture. In addition, global soil moisture data from the NASA–USDA dataset are provided in Fig. 5 as a complementary source to the satellite-derived SMAP data.

The SMAP observations indicate that both surface and sub-surface soil moisture exhibited relatively minor fluctuations over the study period and showed a strong degree of correlation. Consistently, the NASA–USDA soil moisture data indicate predominantly near-normal moisture conditions (values close to zero), with positive and negative anomalies representing wetter and drier soil conditions, respectively. Overall, these results suggest that despite slight variations, soil moisture conditions in the study area have remained relatively stable over the past decade.

Pre-publication Version

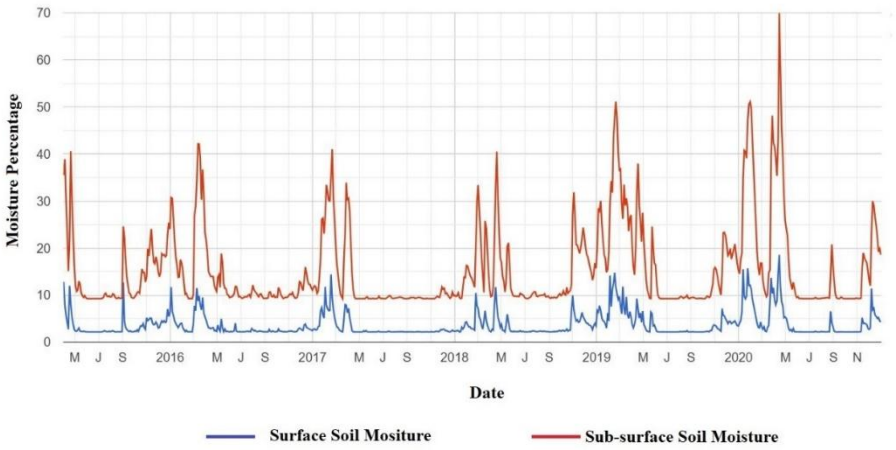


Fig 4. SMAP satellite surface and sub-surface soil moisture percentage in the study area.

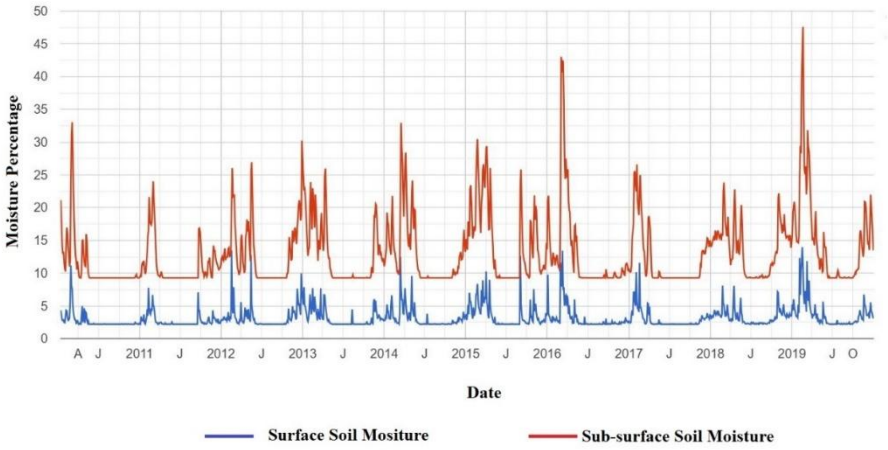


Fig 5. Global NASA-USDA surface and sub-surface soil moisture percentage in the study area.

Pre-publication

Vegetation Indices Analysis

In this part, the results derived from the analysis of various vegetation indices are presented and discussed. As demonstrated in the preceding part, the evaluation of climatic–meteorological variables revealed the occurrence of a meteorological drought in the study area. Therefore, the assessment of vegetation indices over the study period enables the determination of the impacts of this drought on the vegetation cover of this region.

The temporal trends of the NDVI index and green vegetation cover area in the Darmian and Sarbisheh Protected Area during the period 2000–2022 are illustrated in Figures 6 and 7. It should be noted that the green vegetation cover area was derived through thresholding of NDVI images. For this purpose, NDVI values ranging from 0.1 to 0.5, representing sparse natural vegetation (Jiang et al., 2006) as opposed to agricultural vegetation, were classified and extracted as green vegetation cover area.

The graphs presented in Figures 6 and 7 demonstrate a slight yet consistent increasing trend in this index, as indicated by the positive slope of the trend line. Although dense vegetation areas such as agricultural fields were largely excluded through NDVI thresholding, agricultural areas were additionally identified using Google Earth imagery and manually removed from the study region to further improve the accuracy of the analysis. The indices were then recalculated, yielding similar results. This finding suggests that the observed increase in vegetation cover is primarily attributable to natural vegetation, and that agricultural fields—mainly located around villages within the region—do not exert a significant influence on the results.

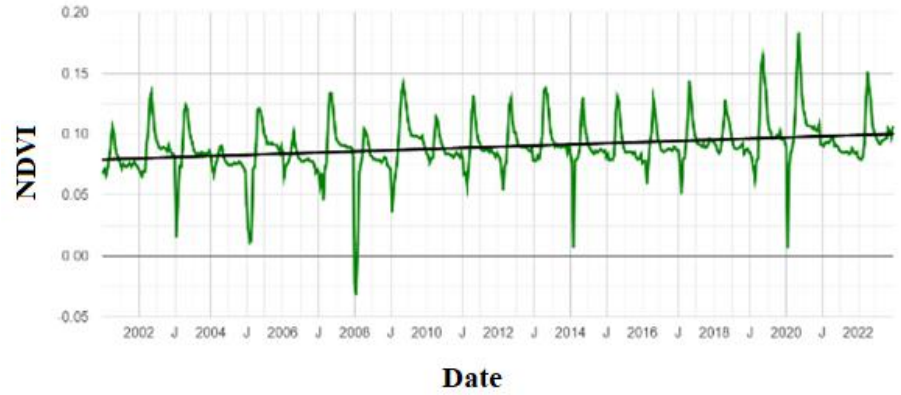


Fig 6. Time series of NDVI over the study area from 2000 to 2022.

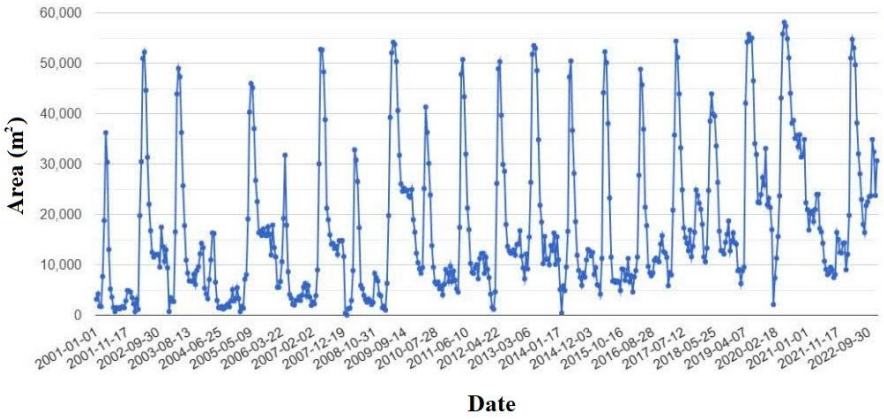


Fig 7. Time series of vegetation cover area within the study area, estimated using NDVI thresholding.

The Mann–Kendall test was also applied to evaluate the presence of a monotonic trend in the vegetation cover area time series (Fig 7). The test produced a Mann–Kendall statistic of $S = 34{,}039$ with a variance of $\mathrm{Var}(S) = 14{,}437{,}445$, resulting in a standardized test statistic of $Z = 8.96$. The associated p-value was effectively zero. ($p < 0.001$), indicating that the null hypothesis of no monotonic trend can be rejected at conventional significance levels. The positive value of Kendall's rank correlation coefficient ($\tau = 0.266$) further confirms a consistent upward tendency in the data. These results demonstrate a statistically significant increasing trend in vegetation cover area over the study period.

To quantify the magnitude of this trend, Sen's slope estimator was also computed. The estimated Sen's slope is approximately 27.26 area units per observation step, indicating that the vegetation cover area increased by about 27.26 units between successive observations on average. Sen's slope is a robust, non-parametric estimator that is resistant to outliers and does not assume a particular distribution of the data. The positive slope value therefore indicates a steady increase in vegetation cover throughout the study period, providing a quantitative measure of the rate of change that complements the statistical significance detected by the Mann–Kendall test.

The temporal trends of the remaining indices are illustrated in Figure 8. The VCI trend line indicates a slight increase (approximately 0.1) in vegetation moisture over the 22-year study period, reflecting an overall improvement in vegetation conditions. The trend of the TCI shows a minor decrease in dryness over time, suggesting increased vegetation moisture during the study years, which is consistent with the VCI trend. Moreover, as expected, the VHI trend line also exhibits an upward trajectory, indicating an overall improvement in the combined behavior of the VCI and TCI over time and suggesting that vegetation conditions remained stable or may have improved during the period of meteorological drought. The SVI, which is similar to the VCI and represents internal vegetation moisture and plant health, further supports these findings. Trend analysis of the SVI reveals that the highest index values occurred in 2019 and 2021, indicating a relative improvement in vegetation conditions based on this index as well.

Pre-Publication

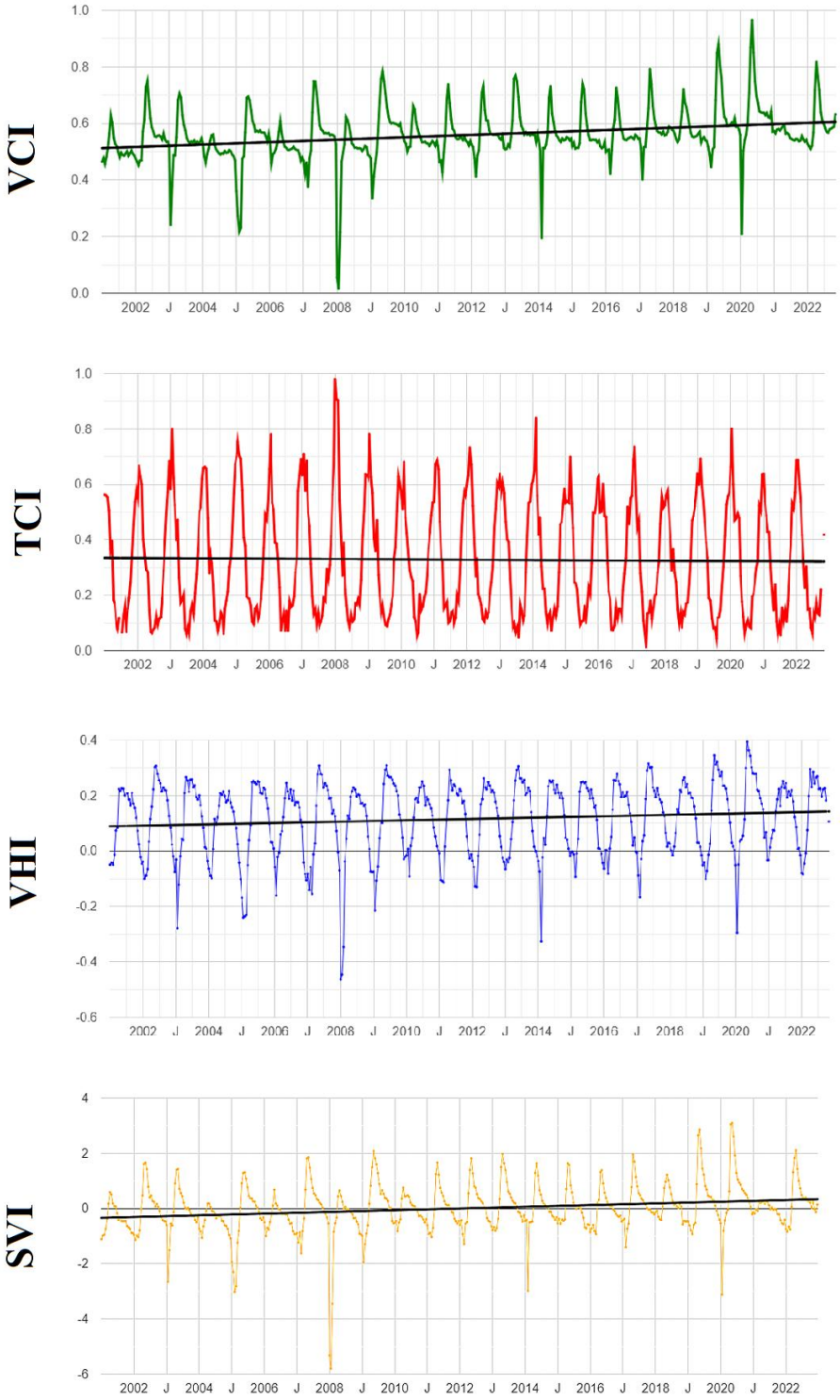


Fig 8. Temporal trends of vegetation indices VHI, VCI, TCI, and SVI across the study area.

Table 3 presents the Mann–Kendall test and Sen's slope estimation results for temporal trends in the vegetation indices VHI, VCI, TCI, and SVI. The analysis shows that SVI, VCI, and VHI exhibit significant increasing trends over the study period, whereas TCI does not show a statistically significant trend. Positive Mann–Kendall statistics (S) and positive standardized test statistics (Z) or SVI, VCI, and VHI indicate upward monotonic trends, with p-values below 0.05 confirming their statistical

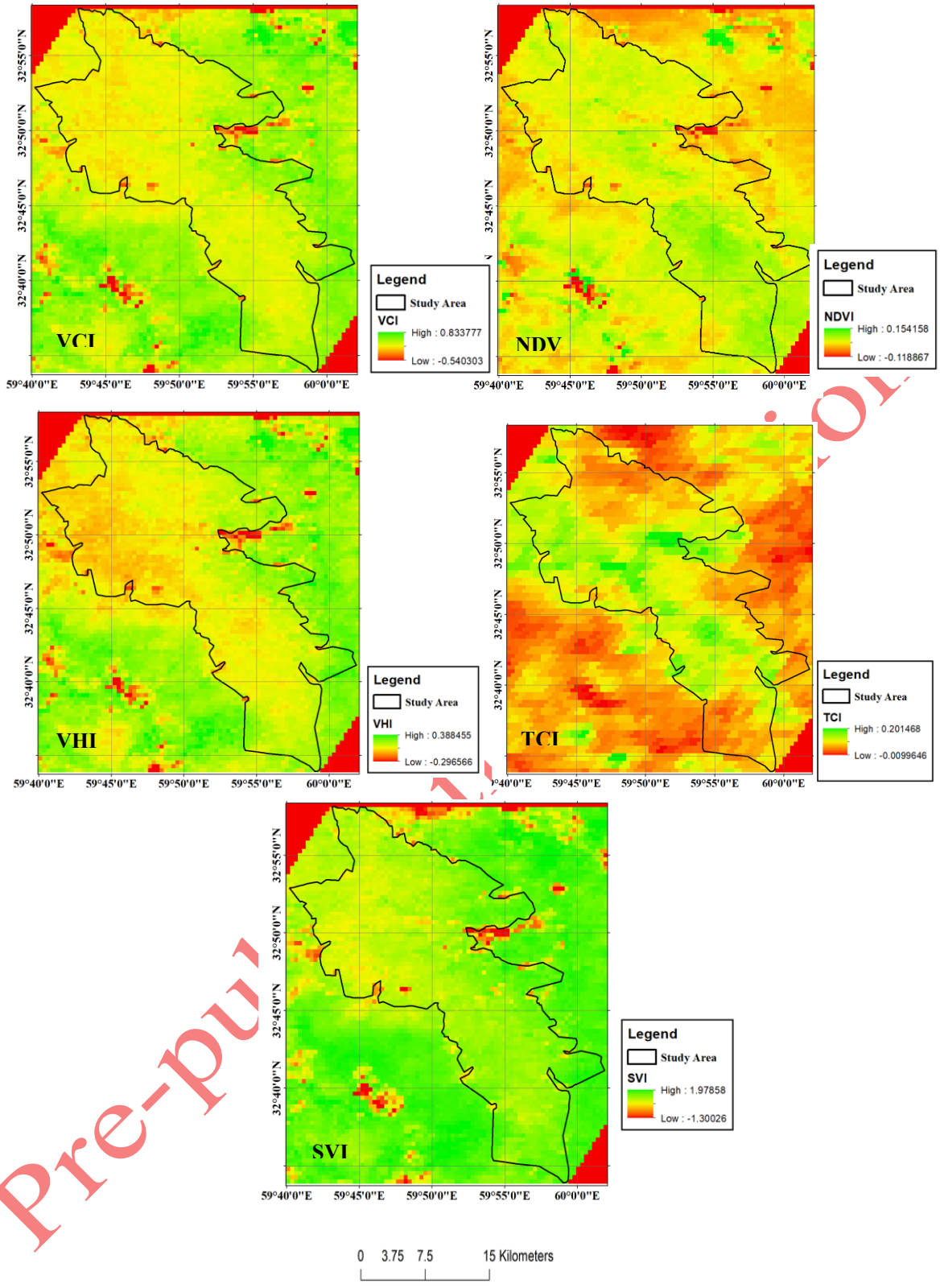
significance. In contrast, TCI has a negative S and Z suggesting a slight decreasing tendency; however, its high p-value ($p = 0.795$) indicates that this trend is not significant.
Among the indices, VCI shows the strongest increasing trend, as evidenced by the largest. S value (30164), the highest Z score (8.009), and the largest Kendall's τ (0.239). SVI also demonstrates a strong and significant upward trend (Z=4.7793, $p \approx 0$, τ=0.142), while VHI shows a weaker but still significant increasing trend (Z=2.402, p=0.016, τ=0.072). The Sen's slope estimates further confirm these results, showing positive slope values for SVI, VCI, and VHI, and a very small negative slope for TCI. Although the slope magnitudes are relatively small, they indicate gradual long-term changes rather than abrupt shifts. Overall, the results suggest that vegetation conditions represented by VCI, SVI, and VHI have improved over time, whereas TCI has remained essentially stable.

Table 3. Results of the statistical test for temporal trends in vegetation indices VHI, VCI, TCI, and SVI.

Statistical parameter	SVI	TCI	VCI	VHI
Mann–Kendall statistic (S)	18161	-973	30164	8995
Variance of S	14437495	14014344	14183358	14014521
Standardized test statistic (Z)	4.779	-0.259	8.009	2.402
p-Value	~0	0.795	~0	0.016
Kendall's rank correlation coefficient (τ)	0.142	-0.007	0.239	0.072
Sen's Slope	9.9×10^{-4}	-1.3×10^{-5}	1.5×10^{-4}	8.1×10^{-5}

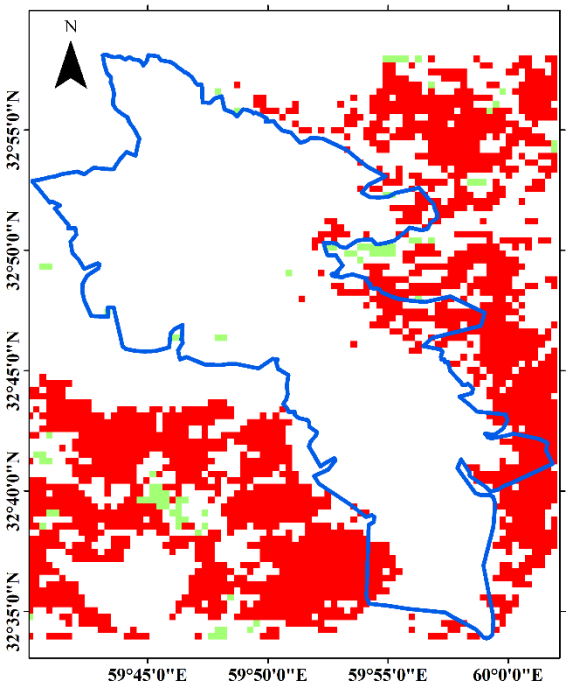
Following the analysis of temporal trends in various indices, as shown in Figure 9, spatial difference maps were generated to better understand the spatial patterns of vegetation changes. These maps were derived by calculating the pixel-wise difference between the vegetation index maps of 2000 and 2022, where positive values indicate net increases in biomass and negative values denote degradation. As illustrated in Figure 9, Examination of these maps indicates that, overall, the indices remained relatively stable, with some areas exhibiting slight positive changes reflecting improved vegetation cover and reduced drought impact. Furthermore, a comparative analysis between protected and non-protected zones (inside and outside of the study area) indicates a clear divergence in resilience; areas under conservation management demonstrate significantly lower sensitivity to drought compared to surrounding regions. This suggests that the establishment of protected boundaries acts as a vital buffer, effectively mitigating the cumulative impacts of aridity on vegetation health.

Pre-publication Version

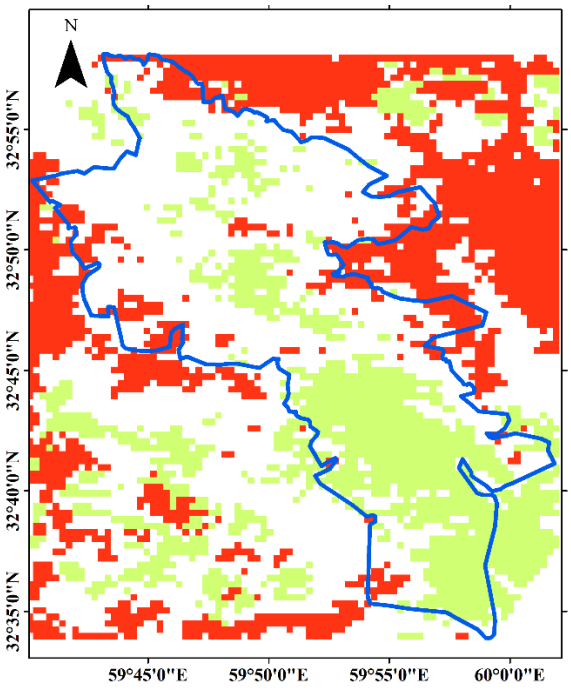


Pre-pu

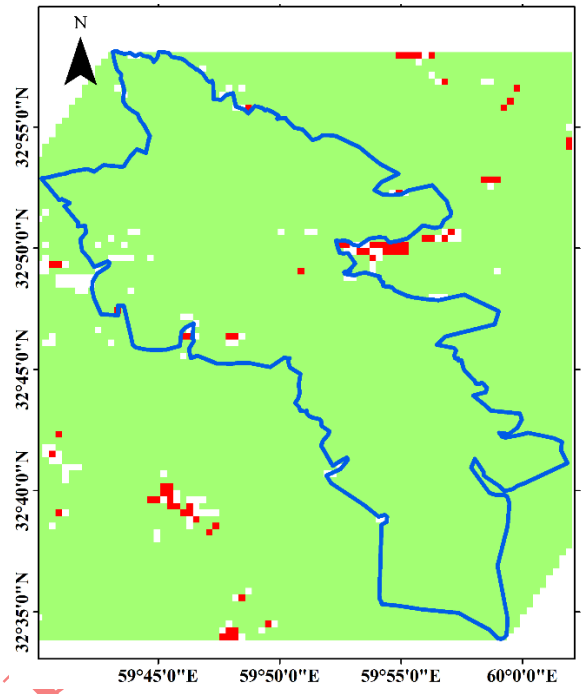
Fig 9. Change maps of vegetation indices—NDVI, VCI, TCI, VHI, and SVI- for the study area, derived by differencing vegetation index maps from 2000 and 2022.



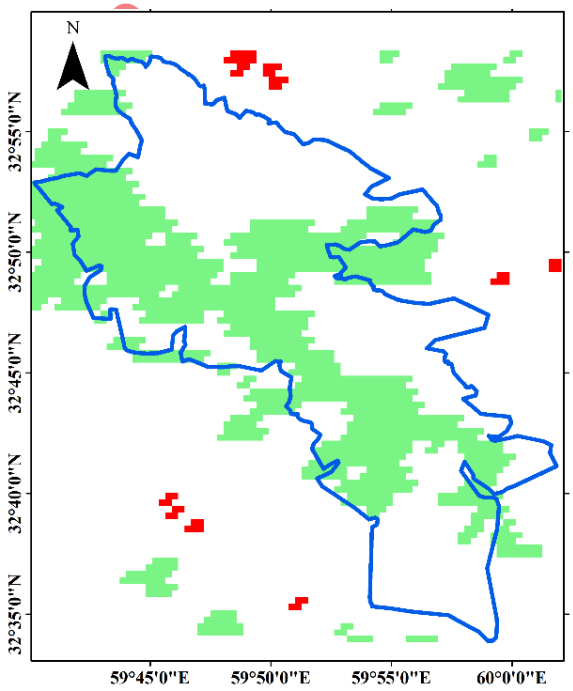
VCI



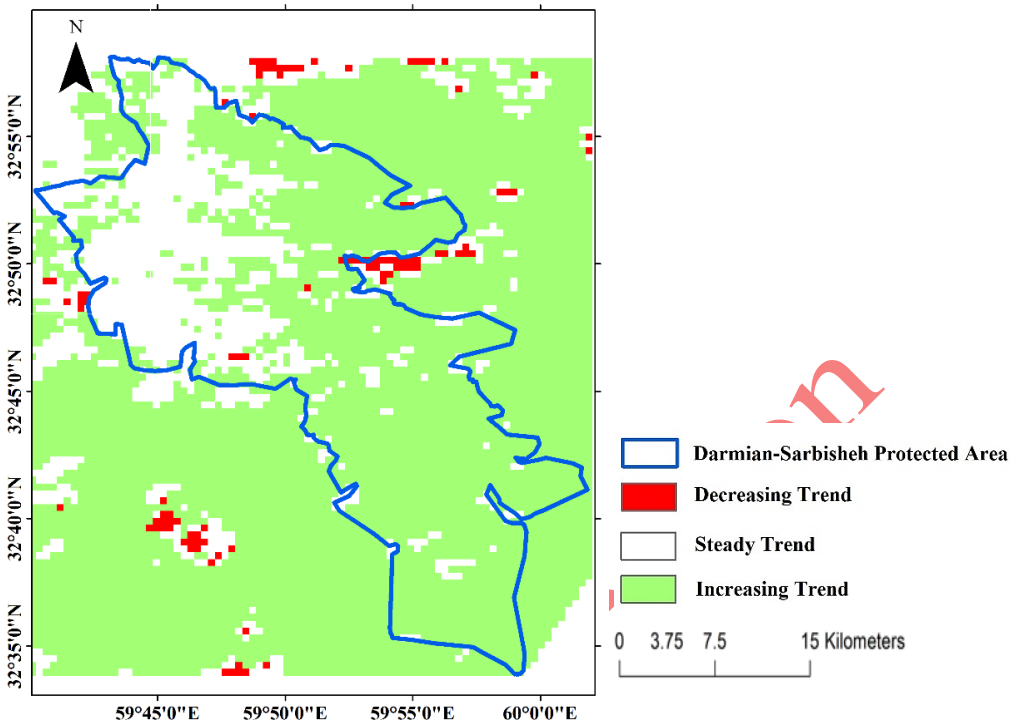
NDVI



VHI



TCI



SVI

Fig 10. Change classified maps of vegetation indices—NDVI, VCI, TCI, VHI, and SVI—for the study area, derived by thresholding difference maps of vegetation indices from 2000 and 2022.

Finally, by thresholding the maps presented in Figure 9, classified maps of vegetation cover changes were produced, as shown in Figure 10. Based on the discussion of Figure 9 regarding the role of conservation management in mitigating the impacts of drought, the maps in Figure 10 provide a clearer illustration of this effect. The classified change maps provide valuable evidence for evaluating the effectiveness of protected-area management in the context of long-term environmental change. By simplifying continuous index differences into meaningful change classes, Figure 10 allows for a more direct comparison of areas experiencing vegetation decline, stability, or improvement.

Examination of these maps indicates that, despite a decline in vegetation cover outside the study area, the trend of vegetation cover inside the protected area has been either stable or increasing—except for the TCI, whose inverse trend actually reflects an increase in vegetation cover. The Mann–Kendall test applied to the vegetation cover area time series indicated a statistically significant increasing trend ($Z = 8.96$, $p < 0.001$, $\tau = 0.27$), while Sen's slope estimated an average increase of 27.26 area units per observation over the study period. This increasing trend was also reflected in the vegetation index time series. This spatial contrast between the protected area and its surroundings suggests that management interventions may have played an important role in enhancing vegetation resilience under drought conditions. Protected areas are commonly associated with reduced anthropogenic pressures, such as overgrazing, land conversion, fuelwood collection, and uncontrolled resource extraction, all of which can intensify vegetation degradation during dry periods. Therefore, the relatively stable or improving vegetation conditions observed within the protected boundary may be attributed to the combined effects of habitat protection, regulated land use, and reduced human disturbance. In contrast, areas outside the protected zone appear to be more vulnerable to drought-induced vegetation loss, likely due to higher exposure to human activities and weaker management controls.

Conclusion

In this study, remote sensing indices—including NDVI, VCI, TCI, VHI, and SVI—derived from MODIS satellite imagery, along with the SPI index from CHIRPS precipitation data, were analyzed in GEE for the Darmian and Sarbisheh Protected Area over the period 2000–2022. The results indicated that, while the SPI exhibited a declining trend over the past two decades—reflecting the occurrence of

Pre-publication

meteorological droughts in the region—the vegetation and agricultural drought indices within the protected area demonstrated stability or slight improvement in natural vegetation cover. This finding highlights the effectiveness of conservation management, grazing restrictions, and control of human activities in mitigating the impacts of drought. In contrast, areas outside the protected zone experienced more severe drought conditions. Soil moisture data, both at the surface and subsurface levels, also indicated slight increases in moisture, consistent with the vegetation drought indices. Comparison of vegetation and drought indices inside and outside the protected area underscores the important role of conservation and management in maintaining vegetation cover and reducing the effects of meteorological drought. Overall, the findings of this study demonstrate that remote sensing indices can effectively reflect the impact of conservation measures in mitigating drought severity in managed areas. Although this study demonstrated the effectiveness of drought indices in environmental research and highlighted the role of management interventions in protecting natural resources, future research could focus on the development of composite indices. For instance, integrating parameters such as evapotranspiration and land surface temperature could yield more comprehensive multivariate indices for improved drought monitoring. Additionally, extending this research to other protected areas would allow for the evaluation of the role of conservation management in controlling drought in similar regions and enable comparative analyses of spatial patterns.

References

Abd-Elhamid, H. F., Zeleňáková, M., Soľáková, T., Saleh, O., & El-Dakak, A. M. (2024). Monitoring flood and drought risks in arid and semi-arid regions using remote sensing data and standardized precipitation index: A case study of Syria. *Journal of Flood Risk Management*, *17*(1), e12961. https://doi.org/10.1111/jfr3.12961

Abonouri, A. A. (2008). Analysis of agricultural drought in Firouzkooh County using water balance method. *Economics of Water*. https://doi.org/10.13031/2013.11223

Alavi-Panah, S. K. (2006). *Application of remote sensing in Earth sciences*. Tehran University Press .

Alipour, H., Chaharsoughi, A., & Gharib, A. (2013). Effects of drought on socio-economic status of farmers: Case study of wheat farmers in Nehbandan County. *Watershed Management Research*, *26*(2), 113–125 .

Alonso, A., Muñoz-Carpena, R., Kennedy, R .E., & Murcia, C. (2016). Wetland landscape spatio-temporal degradation dynamics using the new Google Earth Engine cloud-based platform: Opportunities for non-specialists in remote sensing. *Transactions of the ASABE*, *59*(5), 1331–1342 .https://doi.org/10.13031/trans.59.11608

Bagale, D., Sigdel ,M., & Aryal, D. (2024). Winter drought monitoring using standard precipitation index over Nepal. *Natural Hazards*, *120*(2), 975–988. https://doi.org/10.1007/s11069-023-06242-0

Barrett, A. B., Duivenvoorden, S., Salakpi, E. E., Muthoka, J. M., Mwangi, J., Oliver, S., & Rowhani, P. (2020). Forecasting vegetation condition for drought early warning systems in pastoral communities in Kenya. *Remote Sensing of Environment*, *248*, 111886. https://doi.org/10.1016/j.rse.2020.111886

Bouaziz, M., Medhioub, E., & Csaplovisc, E. (2021). A machine learning model for drought tracking and forecasting using remote precipitation data and a standardized precipitation index from arid regions. *Journal of Arid Environments*, *189*, 104478. https://doi.org/10.1016/j.jaridenv.2021.104478

Delfiyan, F., Yazdanpanah, M., Forouzani, M., & Yaghoubi, J. (2021). Farmers' adaptation to drought risk through farm–level decisions: the case of farmers in Dehloran county, Southwest of Iran. *Climate and Development*, *13*(2), 152–163. https://doi.org/10.1080/17565529.2020.1737797

Du, L., Tian, Q., Yu, T., Meng, Q., Jancso, T., Udvardy, P., & Huang, Y. (2013). A comprehensive drought monitoring method integrating MODIS and TRMM data. *International Journal of Applied Earth Observation and Geoinformation*, *23*, 245–253. https://doi.org/10.1016/j.jag.2012.09.010

Fakhar, M., & Kaviani, A. (2024). Evaluation and Monitoring of Drought in Qazvin Plain Using MODIS-Based Indicators in Google Earth Engine. *Iranian Journal of Irrigation & Drainage*, *17*(6), 1103-1189.

Farajzadeh, M. (2005). *Drought (From Concept to Solutions)* (First ed.). Armed Forces Geographical Organization .

Herring, S. C., Hoerling, M. P., Kossin, J. P., Peterson, T. C., & Stott, P. A. (2015). Explaining extreme events of 2014 from a climate perspective. *Bulletin of the American Meteorological Society*, *96*(12), S1–S172. https://doi.org/10.1175/bams-explainingextremeevents2014.1

Jiang, Z., Huete, A. R., Chen, J., Chen, Y., Li, J., Yan, G., & Zhang, X. (2006). Analysis of NDVI and scaled difference vegetation index retrievals of vegetation fraction. *Remote Sensing of Environment*, *101*(3), 366–378. https://doi.org/10.1016/j.rse.2006.01.003

Jiao, W., Zhang, L., Chang, Q., Fu, D., Cen, Y., & Tong, Q. (2016). Evaluating an enhanced vegetation condition index (VCI) based on VIUPD for drought monitoring in the continental United States. *Remote Sensing*, *8*(3), 224. https://doi.org/10.3390/rs8030224

Pre-Publication Version

Karimi, M., Shahedi, K., Raziei, T., & Miryaghoobzadeh, M. (2020). Analysis of the performance of vegetation indices on agricultural drought using remote sensing techniques in Karkheh basin. *Iranian Journal of Remote Sensing and GIS*, *11*(4), 29–46. https://doi.org/10.52547/gisj.11.4.29
Kogan, F. N. (1995a). Application of vegetation index and brightness temperature for drought detection. *Advances in Space Research*, *15*(11), 91–100. https://doi.org/10.1016/0273-1177(95)00079-t
Kogan, F. N. (1995b). Droughts of the late 1980s in the United States as derived from NOAA polar-orbiting satellite data. *Bulletin of the American Meteorological Society*, *76*(5), 655–668 https://doi.org/10.1175/1520-0477(1995)076<0655:dotlit>2.0.co;2
Kogan, F. N. (1997). Global drought watch from space. *Bulletin of the American Meteorological Society*, *78*(4), 621–636. https://doi.org/10.1175/1520-0477(1997)078<0621:gdwfs>2.0.co;2
Linsley, R. K., & Franzini, J. B. (1981). Water resources engineering (2nd ed.). New York: McGraw-Hill.
Liu, Z. N., Li, Q. F., Nguyen, L. B., & Xu, G. H. (2018). Comparing machine-learning models for drought forecasting in Vietnam's Cai River Basin. *Polish Journal of Environmental Studies*, *27*(6), 2633–2646. https://doi.org/10.15244/pjoes/80866
McKee, T. B., Doesken, N. J., & Kleist, J. (1993, January). The relationship of drought frequency and duration to time scales. In *Proceedings of the 8th Conference on Applied Climatology* (Vol. 17, No. 22, pp. 179-183).
Omidvarpour, F., & Goudarzi, M. R. (2019). Performance of standardized precipitation index in drought forecasting. In *Proceedings of the 3rd Semi-Arid Hydrology Conference: Water, Human, Nature*.
Peters, A. J., Walter-Shea, E. A., Ji, L., Vina, A., Hayes, M., & Svoboda, M. D. (2002). Drought monitoring with NDVI-based standardized vegetation index. *Photogrammetric Engineering and Remote Sensing*, *68*(1), 71–75 .
Qaisrani, Z. N., Nuthammachot, N., Techato, K., & Asadullah. (2021). Drought monitoring based on Standardized Precipitation Index and Standardized Precipitation Evapotranspiration Index in the arid zone of Balochistan province, Pakistan. *Arabian Journal of Geosciences*, *14*(1), 11. https://doi.org/10.1007/s12517-020-06302-w
Quiring, S. M., & Ganesh, S. (2010). Evaluating the utility of the Vegetation Condition Index (VCI) for monitoring meteorological drought in Texas. *Agricultural and Forest Meteorology*, *150*(3), 330–339. https://doi.org/10.1016/j.agrformet.2009.11.015
Rahnama, S., Shahidi, A., Yaghoubi Zadeh, M., & Mehran, A. A. (2022). Assessing drought status using remote sensing, meteorological, and agricultural drought indices in regions with diverse climates. *Iranian Journal of Water and Soil Research*, *53*(10), 2383–2398.
Rashtbari, M., Karimi, N., Shesh Angosht, S., Clorajan, A., & Torabi, O. (2020). Monitoring agricultural drought in arid and semi-arid regions using remote sensing indices. *8th National Conference on Water Resources Management*, Mashhad, Iran.
Rezaei, A., Faridpour, M., Soali, A., & Navidfar, A. (2012). *Monitoring agricultural drought in Urmia Lake basin using remote sensing techniques*. 1st National Conference on Sustainable Development in Agriculture, Natural Resources, and Environment.
Romiyani, S., Gholamrezai, S., Rahimian, M., & Arefnezhad, M. (2020). Analyzing the Agricultural Drought Risk Management Solutions in Lorestan Province: Using Fuzzy Delphi Technique. *Iranian Journal of Agricultural Economics and Development Research*, *51*(1), 65–79. https://doi.org/10.22059/ijaedr.2019.252337.668568
Saedian, A., & Shafiezadeh-Moghadam, H. (2021). Land use change assessment of Karkheh watershed using Google Earth Engine and Landsat images (1990–2020). *Iranian Journal of Water and Soil Research*, *52*(10), 2569–2580. https://doi.org/10.22059/ijswr.2021.330075.669068
Shokrian, F., Solaimani, K., & Darvishi, S. (2022). Investigating agricultural drought changes using remote sensing and meteorological indicators: A case study of North Khorasan Province. *Desert Ecosystem Engineering Journal*, 10(33), 51–65. https://doi.org/10.22052/deej.2021.10.33.51
Suwanlee, S., Keawsomsee, S., Sangjan, W., Som-ard, J., Siripattanachotikul, K., Ninsawat, S., & Nudthawud, H. (2025). Spatio-Temporal Drought Monitoring in the Chi River Basin from 2001–2020 Using MODIS Time Series Data and Google Earth Engine. *International Journal of Geoinformatics*, *21*(1), 43–55. https://doi.org/10.52939/ijg.v21i1.3789
Tabassum, R., & Khan, I. A. (2024). Comparative analysis of drought indices on Google Earth Engine.
Tucker, C. J. (1979). Red and photographic infrared linear combinations for monitoring vegetation. *Remote Sensing of Environment*, *8*(2), 127–150. https://doi.org/10.1016/0034-4257(79)90013-0
Veneros, J., & García, L. (2021). Application of the standardized vegetation index (SVI) and Google Earth Engine (GEE) for drought management in Peru. *Tropical and Subtropical Agroecosystems*, *25*(1). https://doi.org/10.56369/tsaes.3784
Wilhite, D. (2000). Chapter 1: Drought as a natural hazard. *Drought: A Global Assessment*, *1*, 3–18.
Yazdani, V., & Zareh-Abiyaneh, H. S. M. (2011). Frequency and mapping of drought in Iran using standardized precipitation index. *Journal of Water Resources Engineering*, *4*(8), 31–43 .
Zambrano, F., Lillo-Saavedra, M., Verbist, K., & Lagos, O. (2016). Sixteen years of agricultural drought assessment of the BioBío region in Chile using a 250 m resolution Vegetation Condition Index (VCI). *Remote Sensing*, *8*(6), 530. https://doi.org/10.3390/rs8060530

Pre-publication version

Zareh Khormizi, H., & Ghaffarian Malmiri, H. (2020). Examining vegetation phenology components in Iran in response to climate change using AVHRR NDVI (1982–2018). *Remote Sensing and GIS in Natural Resources*, *4*(11), 87–113 .
Zhao, X., Xia, H., Liu, B., & Jiao, W. (2022). Spatiotemporal comparison of drought in Shaanxi–Gansu–Ningxia from 2003 to 2020 using various drought indices in Google Earth Engine. *Remote Sensing*, *14*(7), 1570. https://doi.org/10.3390/rs14071570

Pre-publication Version